Dynamical entanglement and chaos: The case of Rydberg molecules

M. Lombardi and A. Matzkin

Laboratoire de Spectrométrie physique (CNRS Unité 5588), Université Joseph-Fourier Grenoble-1, Boîte Postale 87,
38402 Saint-Martin d'Hères, France

A Rydberg molecule is composed of an outer electron that collides on the residual ionic core. Typical states of Rydberg molecules display entanglement between the outer electron and the core. In this work, we quantify the average entanglement of molecular eigenstates and further investigate the time evolution of entanglement production from initially unentangled states. The results are contrasted with the underlying classical dynamics, obtained from the semiclassical limit of the core-electron collision. Our findings indicate that entanglement is not simply correlated with the degree of classical chaos, but rather depends on the specific phase-space features that give rise to inelastic scattering. Hence mixed phase-space or even regular classical dynamics can be associated with high entanglement generation.

I. INTRODUCTION

Simply stated, a Rydberg molecule is composed of a highly excited electron orbiting around a compact ionic molecular core, containing the nuclei and the tightly bound other electrons. Most of the time, the outer electron is very far from the core. It is spatially well-separated from it, and the core and electron dynamics are uncoupled, the core's dynamics being characterized by its rotational energy. However, the outer electron periodically scatters on the molecular core. In quantum-mechanical terms, the electron and core dynamics get coupled and the collision induces phase shifts in the wave function of the outer electron, known as quantum defects [1,2]. This process has a well-defined classical counterpart [3]: the electron is kicked by the core, resulting in a change of the electron's angular momentum relative to the core by an angle that depends on the quantum defects. During the kick, the core and the outer electron may exchange energy, so that in general the rotational state of the core has changed after the collision. Although a molecule is intrinsically a quantum object, several properties, such as the stroboscopic effect seen in laser excitation or the statistics of the energy levels have been shown to depend on the underlying classical dynamics [3,4].

There is, however, a distinctive quantum feature that has no classical counterpart, which is readily touched upon by observing that a typical molecular state is described by quantum mechanics as a superposition of the different core states available to the molecule, each state being associated with the corresponding outer electron. This superposition is the result of the electron-core entanglement produced by the collision.

The main goal of this paper is to investigate the entanglement dynamics and in particular its dependence on the underlying classical regime. Indeed, there has been a growing interest in recent years to correlate the entanglement production of a quantum system with the dynamics of the corresponding classical system. For example, the time-dependent entanglement production was investigated on the *N*-atom Jaynes-Cummings model (a single mode field interacting with a two-level spin), where the initial product-state wave packet was chosen to lie in different regions of classical phase space [5]. Similar studies were undertaken for kicked tops [6–8]. The initial claims [5,6] by which entanglement would systematically increase with chaos were revised in subsequent works. One of the problems was to unequivocally define the classical counterpart for such systems, which is far from being straightforward for the spin-boson case and has been discussed for the coupled kicks system. A semiclassical approach [9] based on the average properties of phase space concluded that both the coupling strength (in the form of classical correlators) and the global classical dynamical regime were important in understanding the entanglement rate. However, the relevance of universal relations relating the generation of entanglement to the dynamics of the corresponding classical system are still being debated: the form of the initial quantum state is known to play a role [10–12], and from a more general viewpoint realistic systems usually display more complex dynamics than simple systems that present a uniform behavior over all points of phase space. In this respect, the choice of Rydberg molecules to investigate entanglement generation may be fruitful: these real systems are theoretically well described (by quantum defect theory), the semiclassical limit is readily obtained, and the classical dynamics is sufficiently simple to be well understood (at least qualitatively) without being too simplistic.

This work is organized as follows. In Sec. II, we briefly recall some basics concerning the quantum theory of simple Rydberg molecules and describe the classical counterpart of such systems, insisting on the relevant Poincaré surfaces of section. In Sec. III, we determine the degree of the electron-core entanglement, inferred from the linear entropy of the reduced density matrix for the outer electron. We will calculate some simple statistics on groups of eigenstates corresponding to different classical regimes. We will then follow the time evolution of the entanglement from an initially unentangled product state. This will be done for different initial states and various dynamical regimes. The results will be discussed in Sec. IV. We will see that the classical dynamics is reflected in the entanglement generation, but the global dynamical regime is less important than the specific classical effects that are quantum mechanically translated into superpositions. Our closing comments will be given in Sec. V.

II. RYDBERG MOLECULES—QUANTUM AND CLASSICAL

A. Quantum phase shifts

A Rydberg molecule is composed of two elements: a highly excited electron (the Rydberg electron) on the one hand, and the ionic molecular core, positively charged, containing the nuclei and the tightly bound other electrons on the other hand. The Rydberg electron is usually far from the core and only senses the long-range Coulomb field produced by the core, irrespective of the complex interactions involving the core particles. The total energy of the molecule E is consequently partitioned between the energies of the core and of the Rydberg electron.

For definiteness, we will take a diatomic molecule for which vibration can be neglected: rotation is then the only motion available to the core. Since the molecule is isolated, the total angular momentum J and its projection M on an axis fixed in the laboratory are conserved. We have

$$\mathbf{J} = \mathbf{N} + \mathbf{L}, \tag{1}$$

i.e., $\mathbf{J}$ results from the addition of the angular momenta of the core, $\mathbf{N}$, and of the Rydberg electron $\mathbf{L}$. We shall assume that L is conserved, as is often the case, and the standard addition of angular momenta gives

$$|J - L| \le N \le |J + L|. \tag{2}$$

Each state of the core is therefore labeled by $|N\rangle$. Recall that it also follows from the addition of angular momenta that whereas N and L are well defined, their projections M_N and m on the reference axis are not, since only the total projection $M = M_N + m$ is well defined. Therefore, the notation $|N\rangle$ also contains the angular state of the Rydberg electron, via the geometrical angular momenta couplings. As is well known, the energy of the core E^+ depends on N through a rotational constant B_r,

$$E_N^+ = B_r N(N+1), \tag{3}$$

and the total energy of the molecule is thus

$$E = B_r N(N+1) + \epsilon_N, \tag{4}$$

where ϵ_N is the energy and ν_N the effective quantum number of the Rydberg electron,

$$\epsilon_N = \frac{-1}{2\nu_N^2} \tag{5}$$

(atomic units are used throughout). Note that for a given value of E, ϵ implicitly depends on the state of the core: the electron is more or less excited depending on whether the core has a large or small rotation number N. Here we will only deal with bound states (i.e., E is below the lowest ionization threshold). The wave function corresponding to the Rydberg electron in the Coulomb field of a core in the rotational state $|N\rangle$ is thus

$$\phi_N(E,r) = |N\rangle f_L(E - E_N^+, r), \tag{6}$$

r being the radial coordinate and f_L the Coulomb function regular at the origin.

Now when the electron significantly approaches the core, the interaction between the core particles and the electron cannot be neglected. These interactions are embodied in the short-range potential V, which is negligible beyond the core radius r_0. Thus the total Hamiltonian of the molecule is

$$H = H_0 + V, \tag{7}$$

with the functions ϕ_N being eigenstates of H_0. From scattering theory, it is well known that the wave functions for H are obtained from

$$\psi_N(E,r) = \phi_N(E,r) - \sum_{N'} g_L(E - E_{N'}^+, r)|N'\rangle K_{N'N}, \tag{8}$$

where g_L is the Coulomb function irregular at the origin and K is the scattering matrix; $K_{N'N}$ gives the transition probability amplitude between states ϕ_N and $\phi_{N'}$ during the collision. The eigenfunctions of the total Hamiltonian H are obtained by the superposition

$$\psi(E,r) = \sum_N Z_N(E)\psi_N(E,r). \tag{9}$$

The coefficients $Z_N(E)$ are obtained from quantum defect theory [2] by imposing the appropriate boundary conditions at infinity, yielding also the discrete eigenvalues E. We thus see from Eqs. (8) and (9) that a generic wave function for a molecular Rydberg state involves a superposition of core states with different rotational numbers. This is caused by the short-range potential V that transforms the *product state* ϕ_N [Eq. (6)] into the *entangled state* ψ. In practical computations, Eq. (9) is of awkward use because taken individually each of the functions $\psi_N(E,r)$ diverges radially. Equation (9) is therefore rewritten as

$$\psi(E,r) = \sum_N B_N(E)F_L(\epsilon_N, r)|N\rangle, \tag{10}$$

where the $F_L(\epsilon_N, r)$ are the effective channel functions,

$$F_L(\epsilon_N, r) \equiv \sin\beta(\epsilon_N)f_L(\epsilon_N, r) - \cos\beta(\epsilon_N)g_L(\epsilon_N, r), \tag{11}$$

which by construction converge as $r \to \infty$. $\beta(\epsilon_N) \equiv \pi(\nu_N - L)$ is precisely the total phase accumulated at $r \to \infty$. The coefficients B_N are obtained from the Z_N by matching Eqs. (9) and (10).

An additional subtlety arises from the use of frame transformations: the wave functions given above were described in the laboratory frame. However, when the electron collides on the core, a description in the molecular frame, attached to the core rotation, is more appropriate, because in the core region the Rydberg electron senses the cylindrical field aligned along the molecular axis. Thus only the projection of $\mathbf{L}$ on that axis, traditionally denoted by Λ, matters when describing the collision: the phase shifts induced by the collision on the Rydberg electron's wave function are known as quantum defects and denoted by μ_Λ. The collision matrix K appearing in Eq. (8) is obtained by expressing the phase shifts μ_Λ in the laboratory frame [1].
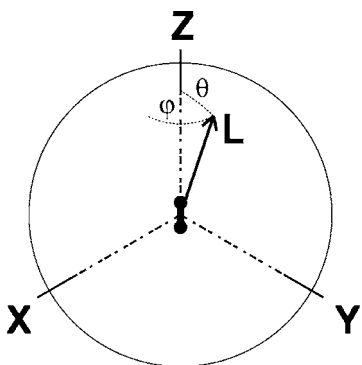
FIG. 1. Molecular reference frame. The core axis is along OZ and its angular momentum **N** is along OX.

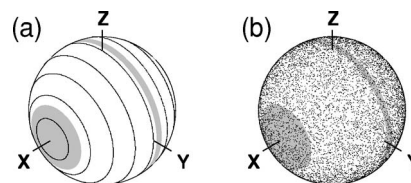
FIG. 2. Two limiting Poincaré surfaces of sections. (a) No coupling $k=0$, (b) large coupling $k=10$ (in the generic case, see Fig. 4 below). The shaded areas correspond to quantum states with minimal ($J-L=40$) and mean ($J=50$) values of N (see Sec. III). Their widths correspond to $\Delta N=1$. The mean $N=J$ case is not on the equatorial OYZ plane, as can be understood by squaring **J**=**L**+**N** (where **N** is "horizontal," parallel to OX) when the lengths of N and J are equal.

B. Classical kicks

The classical counterpart of the quantum model introduced above is the following [3]. When the Rydberg electron is far from the core, it follows a pure Coulomb (Kepler) orbit with an angular momentum **L** fixed in space. Meanwhile, the molecular core rotates freely with a rotational energy $N(N+1)/2I$ depending on the core's angular momentum N and moment of inertia $I=1/2B_r$. Seen in the molecular frame, **L** precesses around **N**, i.e., it turns around the **N** axis with a constant angle (see Fig. 1). Now when the outer electron approaches the core, it gets kicked by the molecular axis. This kick results in a change in the direction of **L**. **N** adjusts accordingly, since the total angular momentum **J** is conserved. To visualize the effects of the kick, it is therefore sufficient to follow the evolution of **L** in the molecular frame.

Since during the collision the Rydberg electron feels the cylindrical field due to the molecular axis, θ cannot change and thus only the angle φ varies (see Fig. 1). This variation, denoted $\delta\varphi$, is the deflection angle of the plane of the classical Kepler orbit. The relation between the classical deflection angle and the quantum scattering phase shifts is well known from the semiclassical approximation to the scattering amplitude [13]. Here it takes the form

$$\delta\varphi = 2\pi \frac{\partial \mu_\Lambda}{\partial \Lambda}, \qquad (12)$$

i.e., the strength of the kick, reflected in the amplitude of the deflection angle, is the classical counterpart of the dependence of the phase shifts on Λ. The precise form of this dependence depends on the particular molecule at hand. However, for a typical molecule, the dependence can be taken in the form

$$\mu_\Lambda = \mu_0 - k \frac{\Lambda^2}{4\pi L}. \qquad (13)$$

Classically, the coupling parameter k gives the strength of the kick since it follows from Eqs. (12) and (13) that

$$|\delta\varphi| = k \frac{\Lambda}{L} = k \cos\theta. \qquad (14)$$

To visualize the classical dynamics, a Poincaré surface of section is obtained by plotting the position of **L** after each kick. This is most naturally done in the molecular frame where the position of **L** is given by the polar angles (θ, φ), as shown in Fig. 1, with φ being canonically conjugate to L_z. This is the molecular reference frame used in quantum mechanics. However, as in our previous works [3,4,14], we prefer to add an extra rotation around OZ to bring the OX axis along **N**. This last rotation is not canonical but the classical motion is seen more naturally in this frame (see the discussion in Ref. [14]). The position of **L** is thus plotted after each kick, when the electron comes out of the core. Of course, since **J**=**L**+**N** is conserved, following the position of **L** is tantamount to knowing the fate of **N**. Two extreme examples of Poincaré sections are given in Fig. 2. In the first case, Fig. 2(a), the positions of **L** follow circles around **N** (the X axis) giving an overall regular surface of section. This means that on a given circle **L** is fixed in space, as is **J**, and thus that $N=|\mathbf{J}-\mathbf{L}|$ is constant. In the second case, Fig. 2(b), the surface of section is clearly characteristic of a chaotic phase space and no structure arises by following the successive positions of **L** after each kick.

III. ENTANGLEMENT DYNAMICS

A. General remarks

Generically, in a Rydberg molecule the core and the outer electron are entangled; in the situation examined in this work, the core is in a superposition of different rotational states. Each rotational state is defined by a given value of N, and to each core state is associated an outer electron with an energy $\epsilon(N)$ given by Eq. (4). Hence the outer electron is in a superposition of different channels that are distinguished in the present model by a different energy, depending on N. Classically of course there is no superposition in N: the rotational energy of the core, and thus the energy of the outer electron, is at each instant unique and well defined. A change in N can only be the dynamical result of an inelastic kick. Note that classically as well as quantum mechanically, the angular momenta **L** and **N** are coupled, since **J** is conserved. As is well known, the composition of angular momenta in quantum mechanics results in couplings due to the fact the projections of the angular momenta vectors cannot be simul-

taneously defined. This entanglement of a geometrical nature (as in EPR pairs) should not be confused with the dynamical entanglement generated by the potential interaction between the outer electron and the core. Geometrical entanglements due to angular momenta coupling do not play any role in this work, as we are only interested in the dynamical one, which only depends on $|\mathbf{N}|$. This implies that a product state is given by the channel functions $\phi_N(E, r)$, defined by Eq. (6), i.e., only the *radial* coordinate of the outer electron is separable from the core whereas its orbital angular momentum is necessarily geometrically coupled to the core's angular momentum $\mathbf{N}$ (since $\mathbf{J}$ is conserved and H_0 has spherical symmetry). Hence when referring to partial traces on the outer electron, we will mean a trace over its sole radial coordinate, and conversely a partial trace over the core includes tracing over the angular coordinates of the electron.

To quantify entanglement we will determine the linear entropy S_2 associated with the reduced density matrix ρ_e describing the outer electron,

$$\rho_e = \mathrm{Tr}_c \rho = \sum_N \langle N | \rho | N \rangle, \tag{15}$$

where $\rho \equiv |\psi\rangle\langle\psi|$ is the density matrix of the system and Tr_c (Tr_e) refers to averaging over the core (outer electron) degrees of freedom. The reduced linear entropy is then defined by

$$S_2 = 1 - \mathrm{Tr}_e \rho_e^2. \tag{16}$$

Strictly speaking, S_2 measures the degree of mixedness: S_2 vanishes for a pure state and is maximum for a uniformly mixed state. However, when S_2 is associated with improper mixtures in bipartite systems, it reflects the degree of entanglement [15], and the linear entropy or equivalent quantities such as the purity have routinely been employed as such [5,7,9–11,16]. We will undertake two different studies. First we will investigate the degree of entanglement on stationary states and its dependence on the collision phase shifts, whose classical counterpart gives rise to different dynamical regimes. This involves the computation of simple statistics of $S_2(E)$ in an energy range for which the classical dynamics does not vary. We will then investigate the time evolution $S_2(t)$ from an initially (at $t=0$) product state. This involves the determination of wave-packet dynamics. The initial wave packet can be made to lie and then evolve in zones corresponding to different classical dynamics.

We will obtain numerical results for the following choice of parameters: $J=50$, $L=10$ yielding by Eq. (2) 21 values for N. Since Kronig's parity, i.e., parity by reflection at a plane through the internuclear axis OZ (which for fixed L and J depends on the parity of N), is conserved, entanglement only takes place between states of the same Kronig parity. States of $(+)$ and $(-)$ Kronig's parity, called positive and negative states in standard spectroscopic notation [17], behave in the same way, and we will restrict our study to $(+)$ parity states; then N can only take even values, so that a typical state contains superpositions involving up to 11 values of N. These angular momenta numbers are considerably higher than for typical diatomic molecules (they would better cor-
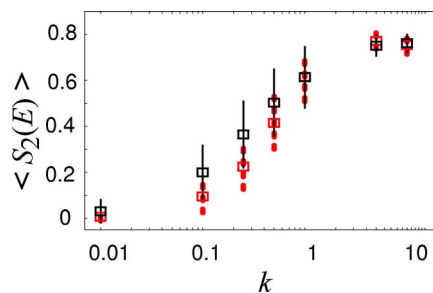

FIG. 3. (Color online) Average linear entropy for generic (red boxes) and resonant $T_e = T_0$ states (black boxes), shown for different values of k. The rms is also shown as red dashed (generic) and solid (resonant) error bars.

respond to models of large molecular compound Rydberg states). However, higher quantum numbers allow a finer comparison between quantum and classical dynamics, without qualitatively affecting the correspondence between them: see [18], where partial results with angular quantum numbers typical of diatomic molecules such as Na_2 were obtained [23].

B. Degree of entanglement of eigenstates

The eigenstates $\psi(E)$ of a Rydberg molecule are given by [Eqs. (10) and (11)]

$$\psi(E) = \sum_N B_N(E)[\sin \beta(E - E_N^+) f_L(E - E_N^+, r)$$

$$- \cos \beta(E - E_N^+) g_L(E - E_N^+, r)] |N\rangle. \tag{17}$$

To quantify the degree of entanglement of a given eigenstate, we compute $S_2(E)$. Variations from individual eigenstates are smoothed out by calculating simple statistics for the bunch of eigenstates sitting in an interval ΔE. The requirement on ΔE is that the classical dynamics does not change appreciably within this interval. Several computations are performed for different values of the coupling constant k. Each value of k corresponds to a different collision matrix K via Eq. (13).

The results are shown in Fig. 3. The average and rms of S_2 are given for different values of k. Figure 3 shows both the results for a "generic" situation which would be obtained for an arbitrary choice of E and the results for resonant eigenstates: in the latter case, E is chosen such that the period of the Rydberg electron T_e is an integer multiple of half the period of the core T_c. Classically, this corresponds to a situation in which the electron sees the core in the same position on its return as when it left the core region. Resonances affect the classical dynamics, essentially by retarding the appearance of chaos. This is portrayed in Fig. 4, which shows Poincaré surface of sections for several values of the coupling k in both the generic and the resonant cases. In the former case, chaos appears even for a small value of k, whereas in the latter configuration, chaos becomes significant for larger values of the coupling, and even for such a large value as $k=10$ an island of regularity around the fixed point on the Z axis is still visible.

Figure 3 indicates that on average the degree of entanglement, as measured by $\langle S_2 \rangle$, increases with k. However, this
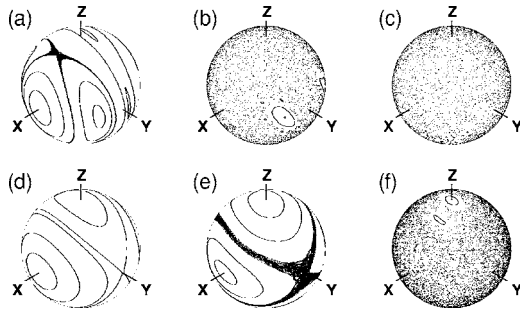
FIG. 4. Poincaré surfaces of section for different values of the coupling constant k. Top, generic; bottom, resonant cases. (a,d) k =0.25. (b,e) k=1. (c,f) k=10.

FIG. 6. Husimi plots (top) and $B_N(E)$ coefficients (bottom) for two particular wave functions in the k=0.5 resonant situation near the center of the interval plotted in Fig. 5. Left level, with $\nu(E)$ =315.4233, is nearly quantized on the minimum value of N=40 as shown by the B_N distribution. Compare its Husimi plot with shaded areas in Fig. 2. It has $S_2(E)$=0.03658. The right level, with ν_E =315.6118, quantized nearby the $+OZ$ axis, spans a greater number of B_N values. Its Husimi plot overlaps with a greater number of N circles indicated in Fig. 2. It has $S_2(E)$=0.6881.

does not mean that entanglement is correlated with classical chaos. Thus, for example for k=0.25, the average entanglement is significantly higher in the resonant case than in the generic case, despite phase space being slightly more regular [see Figs. 4(a) and 4(d)]. For k=1, $\langle S_2 \rangle$ has the same value in the generic and resonant cases, although the dynamical regimes, as reflected in the surfaces of section Figs. 4(b) and 4(e), are quite different.

We further illustrate the effect of a resonance both on the classical dynamics and on the linear entropy for the case k =0.5. Indeed, as the energy is appreciably moved away from the exact resonance energy, the classical dynamics accordingly changes, going back toward a generic situation. This is shown in Fig. 5 (top): the Poincaré surface of section at the center is plotted at the exact resonance energy. However, as the energy changes appreciably, the periods of the Kepler orbit and the core rotation are significantly altered, suppressing the resonance. Classically, the structure of phase space is modified, as can be directly seen on the surfaces of section plotted at both ends of the energy range. At all energies, phase space is regular, but the separatrices characterizing the resonance give way to island chains and curves organized around OX. Figure 5 (bottom) shows the linear entropy for
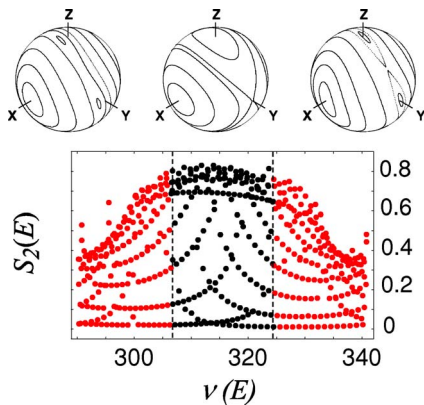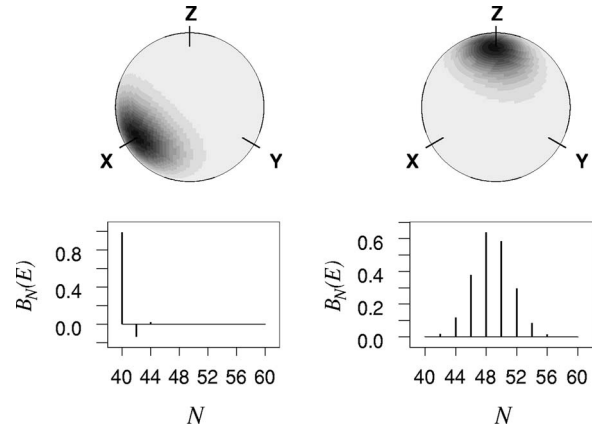

FIG. 5. (Color online) Classical phase-space and linear entropy in the k=0.5 resonant situation. (Top) Poincaré surfaces of sections at the left, middle, and right ends of the energy interval shown at the bottom. (Bottom) Linear entropy of the individual eigenstates. The black dots between the dashed lines correspond to the states that entered the statistics shown in Fig. 3. Each eigenstate of energy E is labeled by $\nu(E)$, the principal quantum number in the N=J channel.

the *individual* states lying within this energy range. It may be seen that as we move away from resonance, the behavior of the linear entropy drops dramatically: most states show a lower degree of entanglement. The degree of entanglement clearly appears to be correlated with the changes in phase space induced by the resonance. The findings presented in Figs. 3 and 5 will be discussed in Sec. IV, but we may note that these results indicate that entanglement is sensitive to the details of classical phase space, not only to the global dynamical regime. Note that the statistics for k=0.5 shown in Fig. 3 were done from the 200 individual states lying within the dashed lines in Fig. 5.

To grasp the relationship between quantum entanglement and the classical dynamics for individual eigenstates, we project the wave functions in mock phase space on the surface of section by drawing the Husimi plots for two eigenstates having different values of S_2. We give in Fig. 6 the Husimi plot along with the 11 B_N coefficients of two particular wave functions lying very near the center of the resonance shown in Fig. 5. The first one is (accidentally) a nearly pure N=40 wave function. Its Husimi plot shows that it is quantized near the $+OX$ axis, as expected from the gray zone displayed in Fig. 2. Being a nearly pure product, it has thus a very low linear entropy, S_2=0.03658. The second wave function is (also accidentally) quantized nearly on the $+OZ$ axis. Its phase-space extension is nearly the same, but the decomposition on the B_N basis spans more values of N, as shown in the lower part of the figure. This is understood by considering the overlap of its Husimi plot with OX-centered circles, each such circle corresponding to a value of N. Its linear entropy is thus correspondingly much higher: S_2=0.6881.

C. Dynamical evolution of entanglement

We consider the time dependence of the generation of entanglement from an initial product state. Assume the sys-

tem has been prepared so that at $t=0$ the core has a well-defined rotational state $|N_0\rangle$ whereas the outer electron is radially localized at the outer turning point of the Kepler orbit, several thousand atomic units away from the core. The wave packet attracted by the Coulomb interaction moves toward the core and collides on it at $t \approx T_e/2$. The collision results in entanglement, since the outgoing waves of the Rydberg electron are in a state of superposition, each outgoing channel being attached to a core in a different quantum state. Subsequent collisions with the core result in further entanglement, whereas the spreading of the radial wave packet quickly results in a continuous core-electron interaction.

We take the initial state to be

$$\psi(t=0,r) = F_{\rm loc}(r \approx r_{tp}) \otimes |N_0\rangle, \tag{18}$$

where the radial function is

$$F_{\rm loc}(r) = \sum_n e^{-[(n-n_0)/2\Delta n]^2} R_{nL}(r) \tag{19}$$

with an appropriate normalization factor. $R_{nL}(r)$ are the standard radial functions of the hydrogen atom (regular Coulomb functions) and the Gaussian form of the coefficients are known to ensure localization [19]. n_0 is chosen so that the central component of the wave packet matches the energy of the corresponding classical regime under study. At later times, the wave function is given by

$$\psi(t,r) = \sum_E \sum_N \mathcal{B}_N(E) e^{-iEt} F_L(E - E_N^+, r) |N\rangle, \tag{20}$$

where

$$\mathcal{B}_N(E) = B_N(E) B_{N_0}(E) \langle F_L(E - E_N^+) | F_{\rm loc} \rangle, \tag{21}$$

where the coefficients $B_N(E)$ and effective channel radial functions $F_L(E - E_N^+)$ were given above [cf. Eqs. (10) and (11)]. The radial overlap $\langle F_L(\epsilon_N) | F_{\rm loc} \rangle$ is determined analytically as a particular instance of the scalar product $\langle F_L(\epsilon) | F_L(\epsilon') \rangle$ given by [20]

$$\langle F_L(\epsilon) | F_L(\epsilon') \rangle = \frac{\sin \pi(\nu - \nu')}{\pi(\nu - \nu')} \tag{22}$$

multiplied by the relevant normalization factors [24].

In principle, the computation of the linear entropy associated with the reduced density matrix is straightforward. From

$$\rho(t) = |\psi(t)\rangle\langle\psi(t)| \tag{23}$$

we obtain the purity $\mathrm{Tr}_e \rho_e^2(t)$ and the reduced linear entropy $S_2(t)$ as

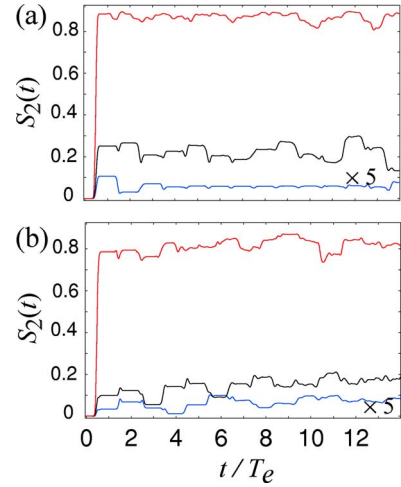$$\mathrm{Tr}_e \rho_e^2(t) = \int \langle r | \rho_e^2 | r \rangle r^2 dr, \tag{24}$$

FIG. 7. (Color online) Short time variation of the linear entropy generated from the initial product state $F_{\rm loc}(r \approx r_{tp}) \otimes |N_0=40\rangle$ for different collision matrices labeled by the value of the coupling strength k: from top to bottom, $k=10$ (topmost curve, red), 1 (middle curve, black), and 0.25 (bottom curve, blue). t is given in units of the Kepler period T_e. (a) The parameters are chosen so that the corresponding classical dynamics falls in the *generic* phase-space case. (b) Same as (a) for the *resonant* case $T_e=T_0$. In both (a) and (b), the $k=0.25$ curve is multiplied by a factor 5.

$$\mathrm{Tr}_e \rho_e^2(t) = \sum_{NN'} \left| \sum_{EE'} e^{-i(E-E')t} \mathcal{B}_N(E) \mathcal{B}_{N'}(E') \right.$$
$$\left. \times \langle F_L(E' - E_{N'}^+) | F_L(E - E_N^+) \rangle \right|^2. \tag{25}$$

The radial closure relation needs to be introduced in Eq. (24) given that the effective radial functions that play the role of the basis are overcomplete.

1. Short-time evolution

We examine first the short-time evolution for three different couplings (kick strength)—$k=0.25$, 1, and 10—and two different initial states distinguished by the value of N_0: $N_0 = J - L$ [that is the minimal value N_0 can take, cf. Eq. (2)] and $N_0 = J$. The corresponding zones in the surfaces of section are shaded in Fig. 2. Recall that on the surface of section, a fixed value of N_0 corresponds to a line circle around the X axis, whereas a quantum state in mock phase space projected on the surface of section has a certain width, as seen in Fig. 6. The width of the initial state can be roughly estimated by plotting the zone going from $N-0.5$ to $N+0.5$, cutting the sphere approximately into the number of values N can take (here 11).

Figures 7(a) and 7(b) show the linear entropy as a function of time (in units of the Kepler period) for the generic and resonant cases when the initial state (18) is chosen with $N_0 = J - L = 40$. Figure 8 gives the linear entropy when the initial state is taken with $N_0 = 50$. In Fig. 7, we observe that in both the generic and resonant cases $S_2(t) = 1 - \mathrm{Tr}_e \rho_e^2(t)$ increases with k: entanglement is produced more rapidly and saturates at a higher value. Comparing with the classical dynamics, we see that in the generic case, the rise in entangle-
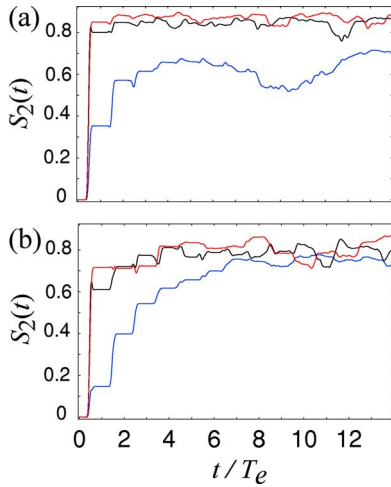
FIG. 8. (Color online) Same as Fig. 7 but with the initial product state given by $F_{loc}(r \approx r_{tp}) \otimes |N_0=50\rangle$ (the $k=0.25$ curve is *not* multiplied by a factor 5).

ment generation accompanies the classical transition to chaos. This remains true to a certain extent in the resonant case, as mixed phase-space turns progressively chaotic.

However, when the initial rotational state lies near the center of the surface of section (Fig. 2), the linear entropy takes very high values irrespective of the classical dynamical regime. This is particularly spectacular for $k=0.25$, which jumps from negligible values in Fig. 7 to crossing the $k=10$ curve of the linear entropy in Fig. 8(b). For the first few periods, this increase of the linear entropy takes place in steps, reflecting the collision of the radially localized electron wave packet with the core at each half-integer value of t/T_e (the wave packet spreads radially after a few periods). These findings will be discussed in Sec. IV, but we may note again that as found for the eigenstates there is no simple relation between the global classical dynamical regime and quantum entanglement generation.

2. Long-time evolution

In Figs. 7 and 8, the linear entropy appears to saturate after a few periods. For longer times $S_2(t)$ is plotted in Figs. 9 (when the initial state has $N_0=40$) and 10 ($N_0=50$). In most of the cases [all the $k=10$ curves and the $k=1$ curves except in Fig. 9(b)], $S_2(t)$ appears to vary randomly around some average value. However, for small kicks [the $k=0.25$ curves, but also the $k=1$ curve in Fig. 9(b)] the repetition of oscillatory structures is clearly visible to the eye. These repetitions are due to partial wave-packet revivals within each channel, which take place when the terms that control the spreading of the packet regain an approximate phase coherence. The revival times within each channel are determined in the semiclassical approximation by expanding the energies in the exponentials in Eq. (25) as a function of the classical action. The core's revival time $T_c^{rev} \propto B_r^{-1}$ is independent of the energy, whereas $T_e^{rev} \propto \epsilon^{-2}$. A revival in the linear entropy will be visible provided one or two channels dominate in the overall contribution.

For the $k=0.25$ case in Fig. 9(b), most of the probability density stays in the original $N_0=40$ channel, a small flux
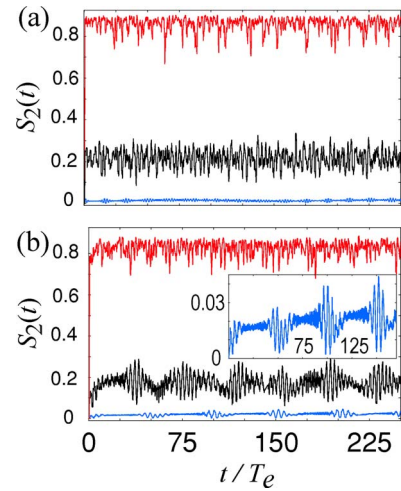
flowing to the $N=42$ channel. This flux is responsible for the main part of the entanglement generation. We have plotted in Fig. 11 the correlation function

$$C(t) = \langle \psi_{42}(t = T_e/2) | \psi_{42}(t) \rangle, \qquad (26)$$

where

$$|\psi_{42}(t)\rangle \equiv \langle N = 42 | \psi(t)\rangle \qquad (27)$$

gives the electronic wave packet in the $N=42$ channel. It can be seen that near $t=100\ T_e$ the correlation function oscillates dramatically: high peaks appear while at the same time the lowest values are near zero. This behavior translates into the entanglement rate, which shows the same strong oscillations as seen in the inset in Fig. 9. The revival time for the electron
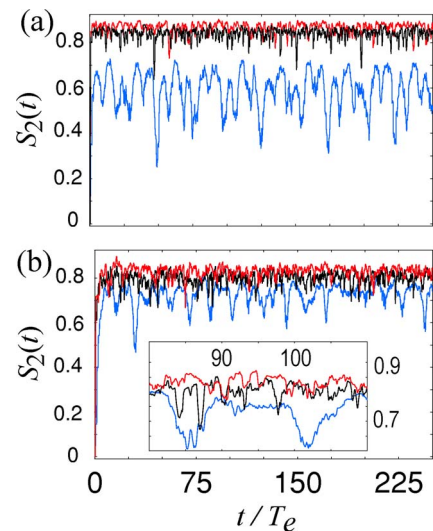

FIG. 9. (Color online) Long-time variation of the linear entropy for the case considered in Fig. 7 [$N_0=40$, (a) generic and (b) resonant cases]. The inset in (b) blows up the vertical scale for the $k=0.25$ curve to help visualize the oscillations, also visible for $k=1$.

FIG. 10. (Color online) Long-time variation of the linear entropy for the case considered in Fig. 8 [$N_0=50$, (a) generic and (b) resonant cases]. The inset in (b) details $S_2(t)$ in the region $t=80$ to $110\ T_e$.
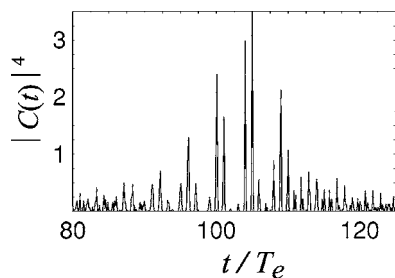
FIG. 11. The partial autocorrelation $C(t)$ defined by Eq. (26) (parameters corresponding to the $k=0.25$ resonant case, arbitrary units) is plotted in an interval centered around the revival time $T_e^{\mathrm{rev}} \simeq 105\, T_e$.

motion in this case is computed in the semiclassical approximation as $T_e^{\mathrm{rev}} \simeq 105\, T_e$. This value fits well with the periodic repetitions of these strong oscillations observed for $S_2(t)$.

IV. DISCUSSION

If we compare the time evolution of the linear entropy portrayed in Fig. 7 to those of Fig. 8, the importance of the initial state is clear. If we further contrast these results with the Poincaré surfaces of section of Fig. 4 and the localization of the initial states shown in Fig. 2, we see that the generation of entanglement does not essentially depend on the global classical dynamics, but rather on the specific dynamics that leads to inelastic scattering. Classically, inelastic scattering means that the value of N changes during the collision; then on the surface of section, two consecutive points cannot lie on circles around the X axis (since these circles correspond precisely to a fixed value of N). Inelastic collisions do take place when the dynamic is chaotic: for very strong kicks ($k=10$), two consecutive points on the Poincaré sections are arbitrarily separated on the sphere. Quantum mechanically inelastic scattering is translated into superpositions of states having a different value of N. The $k=10$ curves in Figs. 7(a) and 8(a) indeed reflect large and fast entanglement generation. $S_2(t)$ achieves its maximal value (of 10/11) just after a couple of collisions.

However, inelastic scattering can also be induced by regular dynamics. Consider $k=0.25$ in the resonant case. When the initial state encircles the X axis at the front of the sphere as happens with $N_0=40$ (see the shaded region in Fig. 2), it will be hardly modified by the classical dynamics. The lines in the surface of section [Fig. 4(d)] also encircle the X axis, thereby conserving N_0: there is essentially only elastic scattering. Quantum mechanically we expect little or no entanglement, as is observed in Fig. 7. But for $N_0=50$, the initial distribution spans across the lines of regularity in the surface of section, which are organized around the elliptic fixed point on the Z axis. These lines thus define torii in phase space that cut across several values of N, meaning inelastic scattering and quantum-mechanical superpositions. Note that in the generic $k=0.25$ situation, the linear entropy is lower than in the resonant case; classically, the structure of phase space in the zone covered by the initial state is modified due to the appearance of resonant islands [Fig. 4(a)],

leading to some lines that roughly encircle the X axis, partially favoring elastic scattering.

We thus see that the entanglement production reflects the classical dynamics in that the relevant parts of phase space leading to inelastic collisions (yielding quantum superpositions) are explored with a large amplitude. To a large extent, this phenomenon is unrelated to whether the dynamical regime is chaotic or regular. Classical chaos is not necessary to induce high entanglement generation. In our system chaos is sufficient, because it always leads to inelastic scattering. Hence eigenstates quantized in an underlying strongly chaotic phase space will present on average a large amount of mixtures, as seen in Fig. 3. These remarks are in line with similar conclusions [10–12] that, contrary to earlier results [5,6], do not attribute to chaos a higher entangling power.

Let us mention that more precise investigations of the correlations between classical dynamics and dynamically induced entanglement should take into account more information than what can be inferred from the Poincaré surfaces of sections. For example, in the generic $k=1$ case [Fig. 4(b)], diffusion in the chaotic sea takes place at a considerably lower rate than in the $k=10$ situation. In particular, the particle may be trapped for several periods in certain regions of phase space, diffusing slowly in the relevant regions of the surface of section. This type of phenomenon has an influence on the quantization process, and if important it will influence the entanglement production, as in the present case. We therefore expect that these system-specific features, along with the role of the initial state relative to the precise structure of phase space, may severely constrain the applicability to realistic systems of general "universal" formulas ruling the entanglement generation in chaotic and regular systems that have been recently obtained [9,16]. Semiclassical universal formulas, based on the global average properties of classical phase space, are important as they set the trend that is followed by a quantum system with simple dynamics (like a uniform transition to chaos). However, individual features of the system are known to be important in the semiclassical description of diffractive effects induced by a coupling potential and need to be taken into account, e.g., to describe the spectral statistics [21]. It is thus not surprising to see that dynamical entanglement induced by a standard potential coupling is correlated with the local structure of phase space, and not only with its global properties.

Concerning the long-time behavior, it may be noted that the revivals appear well beyond the Heisenberg time, after which quantum phenomena having no classical counterpart become prominent. In some cases, for example when the number of channels is small, the oscillations due to wave-packet revivals induce very large variations of the entanglement rate totally unrelated to the behavior at short times. Hence the linear entropy of a state that initially only showed a slow and small amount of entanglement generation can rise above the linear entropy of a state that initially displayed high and fast entanglement production.

We finally point out that entanglement in Rydberg molecules is routinely detected experimentally, given that the consequences of entanglement appear in even the most elementary measurements (e.g., interference of Rydberg series in photoabsorption spectra). A quantitative measurement of

entanglement, which would more closely reflect the evolution of the linear entropy, can be set up by combining the methods employed for the detection of interfering Rydberg wave packets [22]. These methods are based on the use of several laser pulses with well-defined phase relations to monitor the interferences appearing in the population of pre-defined Rydberg states.

V. CONCLUSIONS

We have investigated the entanglement production in Rydberg molecules and contrasted the results with the underlying classical dynamics, which is known to play a role in the understanding of observable spectroscopic effects [3] and in the interpretation of the energy levels statistics [4]. We have first determined the average linear entropy of eigenstates corresponding to different collision strengths (quantum phase shifts or classical kicks) and then studied the generation of entanglement from initially unentangled states. We have seen that the quantum/classical correspondence on the level of entanglement production is relevant not on the scale of the global classical dynamical regime, but rather on the specific classical features that quantum mechanically translate into superpositions. In Rydberg molecules, it is a high rate of inelastic scattering for an initial classical distribution that corresponds in the quantum domain to states displaying a high degree of entanglement. The relation between global chaotic or regular behavior on the one hand and these specific classical features that will be translated quantum mechanically as entanglement production on the other hand appears to depend strongly on the individual system under investigation. We therefore conclude that it seems unlikely that the generation of entanglement could be employed as a reliable signature of chaos for an arbitrary dynamical system.

[1] U. Fano, Phys. Rev. A **2**, 353 (1970).

[2] *Molecular Applications of Quantum Defect Theory*, edited by Ch. Jungen (Institute of Physics, Bristol, 1996).

[3] M. Lombardi, P. Labastie, M. C. Bordas, and M. Broyer, J. Chem. Phys. **89**, 3479 (1988).

[4] M. Lombardi and T. H. Seligman, Phys. Rev. A **47**, 3571 (1993).

[5] K. Furuya, M. C. Nemes, and G. Q. Pellegrino, Phys. Rev. Lett. **80**, 5524 (1998).

[6] P. A. Miller and S. Sarkar, Phys. Rev. E **60**, 1542 (1999).

[7] H. Fujisaki, T. Miyadera, and A. Tanaka, Phys. Rev. E **67**, 066201 (2003).

[8] J. N. Bandyopadhyay and A. Lakshminarayan, Phys. Rev. E **69**, 016201 (2004).

[9] Ph. Jacquod, Phys. Rev. Lett. **92**, 150403 (2004); **93**, 219903(E) (2004).

[10] R. Demkowicz-Dobrzanski and M. Kus, Phys. Rev. E **70**, 066216 (2004).

[11] T. Gorin and T. H. Seligman, Phys. Lett. A **309**, 61 (2003).

[12] H. Fujisaki, Phys. Rev. A **70**, 012313 (2004).

[13] K. W. Ford and J. A. Wheeler, Ann. Phys. (N.Y.) **7**, 259 (1959).

[14] B. Dietz, M. Lombardi, and T. H. Seligman, Ann. Phys. (N.Y.) **312**, 441(2004).

[15] B. d'Espagnat, *Conceptual Foundations of Quantum Mechanics* (Perseus, New York, 1976).

[16] M. Znidaric and T. Prosen, Phys. Rev. A **71**, 032103 (2005).

[17] G. Herzberg, *Molecular Spectra and Molecular Structure. I. Spectra of Diatomic Molecules*, 2nd ed. (Van Nostrand, New York, 1950), p. 217.

[18] M. Lombardi and A. Matzkin, Europhys. Lett. **74**, 771 (2006).

[19] M. Nauenberg, J. Phys. B **23**, L385 (1990).

[20] R. H. Bell and M. J. Seaton, J. Phys. B **18**, 1589 (1985).

[21] A. Matzkin and T. S. Monteiro, Phys. Rev. E **70**, 046215 (2004); J. Phys. A **37**, L225 (2004).

[22] R. R. Jones and L. D. Noordam, Adv. At., Mol., Opt. Phys. **38**, 1 (1998).

[23] In fact, relative to [18] we choose in this work a situation with identical classical parameters (in particular the coupling constant k and the crucial ratio T_e/T_c), and thus identical Poincaré surfaces of sections, but with an effective $\hbar$ divided by 5, and thus all quantum numbers (L, J, N, ν) are multiplied by 5, and B_r is divided by 5^4.

[24] This must be done with care, as Eq. (22) supposes a channel normalization to unity, whereas the MQDT wave functions are normalized globally per unit energy [2,14]. Failure to normalize correctly the radial channel functions F_L results in an imperfect cancellation when taking the scalar product of two different eigenstates, leading to errors of the order of several 10^{-3}. Still perfect cancellation does not occur, as errors due to the approximate nature of MQDT itself remain. These errors are, however, in the fully negligible range $10^{-5} - 10^{-6}$, as we have checked by an independent test calculation that makes an "exact" computation with a given short-range potential.